Draft version November 30, 2021
Typeset using LaTeX default style in AASTeX631

Stellar Peanuts: A Binary Analysis and Period Study of KIC 7766185

Conor M. Larsen[1]

[1] *Department of Astrophysics and Planetary Science*
Villanova University
800 E Lancaster Ave
Villanova, PA, 19085, USA

ABSTRACT

We present the first in-depth photometric and spectroscopic study of the contact binary KIC 7766185. Spectroscopic observations were conducted by the Mayall 4-m telescope at Kitt Peak National Observatory and used to create a radial velocity curve. Using the radial velocity curve and *Kepler* measurements, binary analysis was performed in *PHOEBE* to determine system parameters and the first set of absolute stellar parameters. This study determines values for the mass ratio ($0.835^{+0.067}_{-0.059}$), semi-major axis ($4.97^{+0.19}_{-0.18}$ $R_\odot$), primary mass ($1.29^{+0.19}_{-0.15}$ $M_\odot$), secondary mass ($1.08^{+0.13}_{-0.12}$ $M_\odot$), primary radius (1.99 $R_\odot$), secondary radius (1.83 $R_\odot$), fillout factor (0.0426), inclination (72.5°), and temperature ratio (0.960). The absolute stellar parameters confirm KIC 7766185 as an A-type W UMa system. Along with the binary analysis, a period study was conducted. The O-C diagram determined that there are no current period variations. However, the study demonstrated that the ephemeris reported in the *Kepler Eclipsing Binary Catalog* needs refinement. We report a new value for the ephemeris of KIC 7766185 of 2454954.55433996.

Keywords: W UMa Stars – Absolute Stellar Parameters – Individual: KIC 7766185

1. INTRODUCTION

Contact binaries include some of the most interesting and extreme binary star systems. In these systems, two stars orbit so close that they share a common envelope. Of the contact binaries, the most common type is the W UMa type stars, consisting of two late type stars (mostly of spectral type F, G and K) which have come in contact and share a common, convective envelope (Terrell et al. 2012). The W UMa type stars are low mass and have relatively equal eclipse depths (Eker et al. 2008).

The contact model for W UMa stars was first proposed by L.B. Lucy. His seminal paper, published in 1968, described the first complete theory of contact binaries (Lucy 1968). Since this work, the de-facto explanation for W UMa stars states that the stars come in thermal and geometric contact. The origin and evolution of these objects is still unresolved. However, there is little doubt that angular momentum loss plays a role in formation. The current consensus states that contact binaries were initially detached binaries. Through angular momentum loss, and subsequent orbital decay, the stars migrate towards one another until contact is achieved (Ruciński 1986). The exact mechanism of angular momentum loss is also an open question, however theorists have proposed mass loss via stellar wind, mass transfer and magnetic braking as potential explanations (Ruciński 1986; Gazeas & Stępień 2008).

The stars in contact binaries are so close that tidal distortions become present. Since the stars overflow their Roche Lobes, they are connected via a thin neck through the inner Lagrange point (Csizmadia & Klagyivik 2004). Therefore, contact binaries form a typical "peanut" shape.

Due to the contact between the stellar components, the stars in W UMa systems usually have the same temperature and luminosity, despite having different masses and radii. This property had been noted before the merging nature of contact binaries was realized (i.e., before Lucy's groundbreaking work) (Binnendijk 1965). Once the stars come in geometrical contact, they come in thermal contact with one another (except for B-type W UMa stars, discussed below). Once in thermal contact, thermal energy is transferred between the two stars, forcing the luminosity and temperature of the two objects to become relatively equivalent, within a few hundred kelvin (Csizmadia & Klagyivik 2004).

Parameter	Value	Reference
Distance	$933.881^{+25.168}_{-23.880}$ pc	1
Orbital Period	0.8354573 days	2
$T_{\rm eff}$	5977 K	2
log(g)	4.280 in cgs units	2
E(B-V)	0.077	2
V-Filter Magnitude	12.02 ± 0.18	3
Spectral Type	F3V	4
T_2/T_1	0.97814	5
Mass Ratio	0.81789	5
Fillout Factor	0.18943	5
sin$i$	0.97737	5

Table 1. System Parameters of KIC 7766185. References: 1: *Gaia EDR3*, Brown et al. (2021). 2: *KIC*, Brown et al. (2011). 3: *Tycho-2 Catalog*, Høg et al. (2000). 4: Frasca, A. et al. (2016) 5: Prša et al. (2011)

W UMa stars have 3 sub-types based on temperature and size. A-type systems occur when the larger star is the hotter component, and W-type systems occur when the smaller star is the hotter component (Csizmadia & Klagyivik 2004). B-type systems have much larger temperature differences. B-type W UMa stars are in geometric contact, but not thermal contact which allows the two stars to have vastly different temperatures. Generally, B-type systems are those which have a difference in surface temperature of more than 1000 K (Csizmadia & Klagyivik 2004).

This study focuses specifically on the contact binary KIC 7766185. KIC 7766185 is a $12^{\rm th}$ magnitude system of spectral type F3V (Frasca, A. et al. 2016). Certain parameters for this target were previously determined in large reviews of *Kepler* data (Prša et al. 2011; Frasca, A. et al. 2016), however, there has yet to be an in-depth study focusing specifically on this target. The values presented by Prša et al. (2011) were determined by the EBAI (Eclipsing Binaries via Artificial Intelligence) Estimator (Prša et al. 2008) which is used to estimate system parameters. As will be shown in Section 4, these parameter values do not accurately model the system. A review of previously determined parameters of KIC 7766185 is presented in Table 1. Note that the values for effective temperature and log(g) are weighted averages of the two stars obtained at a random phase. Since the phase is unknown, the contribution of light by each individual star is unknown. Therefore, these values, obtained from the *Kepler Input Catalog* (*KIC*) (Brown et al. 2011), are estimates of the average values of the two stars.

Along with the binary analysis, a period study was conducted on KIC 7766185. The structure and origin of contact binaries are an active area of stellar research. A major theoretical approach to explaining contact binaries is Angular Momentum Loss (AML) (see Gazeas & Stępień 2008; Rucinski 1982). Angular momentum loss by the system can be gauged by period changes. Therefore period studies can determined the overall evolution of the system. Period studies can also indicate whether a contact binary is a red nova candidate. If orbit decay continues after contact is achieved, contact binaries may undergo a full merger (Gazeas et al. 2021). This was the case with V1309 Scorpii, which was a contact binary that underwent orbital decay until merging into a single star, igniting a red nova (Tylenda, R. et al. 2011). Orbital period variations could indicate that the stars are still undergoing orbital decay, making KIC 7766185 a red nova candidate.

This paper will discuss the observations of KIC 7766185 (2), the radial velocity measurements (3), the binary analysis (4), the period study (5) and finally a discussion of the results (6) and a conclusion (7).

2. OBSERVATIONS

2.1. *Photometric Observations*

KIC 7766185 has been extensively observed by the *Kepler Space Telescope* (Borucki et al. 2010). Several measurements were obtained between 2009 and 2013 which were utilized to create a phase folded light curve with a period of 0.835 days. KIC 7766185 was observed in quarters 0 - 17 using the *Kepler* filter which covers a wavelength range of 400 nm - 850 nm. The *Kepler* data was downloaded from the *Kepler Eclipsing Binary Catalog* (Prša et al. 2011). The *Kepler* phase folded light curve is displayed in Figure 1. The light curve has rounded tops, a distinct feature of contact binaries. The primary and secondary eclipses are of relatively equal depth, indicating a temperature ratio close to 1. Since the eclipses are of equal depth and the system consists of late type stars (spectral type of F3V,

Frasca, A. et al. 2016), KIC 7766185 is a W UMa star. Clear outliers are visible in the light curve. Before analysis was conducted, the outliers were removed using the outlier removal function in the period analysis software *Peranso* (Paunzen & Vanmunster 2016). The outlier removal function draws a smooth line through the data along with an envelope with a specified width. All measurements lying outside the envelope are tagged as outliers. Through this method, 323 observations were removed as outliers. Visual inspection of the light curve afterwards verified that the outlier observations had been removed.

KIC 7766185 was also observed by the *Transiting Exoplanet Survey Satellite* (*TESS*) (Ricker et al. 2015). Observations were conducted between July and August 2019 during *TESS* sector 14. During this sector, 28 days of measurements were completed. *TESS* utilizes a red-optical filter covering a wavelength range of 600 - 1000 nm. The binary analysis was conducted with the *Kepler* light curve only since these observations were obtained around the same time as the spectroscopic observations (see section 2.2). The *TESS* measurements were only utilized for the period analysis section.

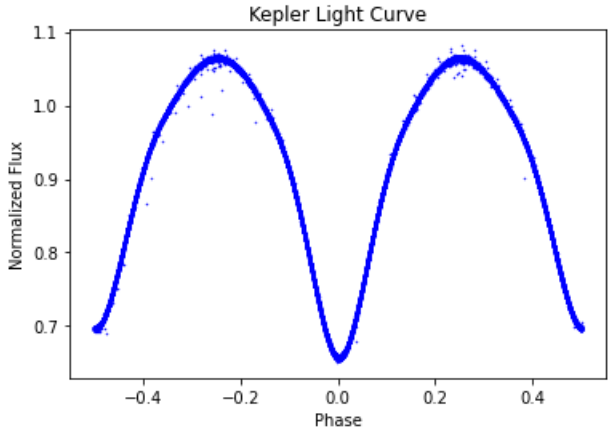

Figure 1. Phase folded light curve of KIC 7766185 created using *Kepler* data

2.2. *Spectroscopic Observations*

Spectroscopic observations of KIC 7766185 were obtained by the Kitt Peak Mayall 4-m telescope located at Kitt Peak National Observatory, Arizona (KPNO 2021). The measurements were obtained during an observing run dedicated to measuring spectra of W UMa type stars identified by *Kepler* (Proposal ID: 2010B-0434). The observations were conducted with a Tektronix 2048x2048 chip (T2KB) and the Echelle spectrograph (31.6 gratings/mm). The data files were obtained from the project PI (Dr. Andrej Prša, Villanova University). A total of 7 spectra were obtained between September 26, 2010 and September 28, 2010. Each spectra was obtained with an exposure time of 600 seconds over a wavelength range of ∼4000 Å to ∼10000 Å. The 4 spectra obtained on September 26 and the one spectrum obtained on September 27 were maintained at a camera temperature of -77 °C. The 2 spectra obtained on September 28 were maintained at a camera temperature of -75 °C. The spectra were reduced through a pipeline before being obtained by the observing run PI. They were reduced in *IRAF* (Tody 1986) using the echelle package (Valdes 1992). The crreject algorithm was used to remove cosmic rays from the data (J. Orosz, personal communication, Nov. 8, 2021). One of the spectra is displayed in Figure 2. The deepest lines visible are due to telluric contamination (i.e., due to interference from the Earth's atmosphere).

Table 2 displays a list of the 7 spectra along with the corresponding Julian date and phase. The phase was calculated using the ephemeris (T_0, in days) and period (P, in days) listed in the *Kepler Eclipsing Binary Catalog* and the observation time for each spectrum (T_{obs}, in days):

$$E = \frac{T_{obs} - T_0}{P} = \frac{T_{obs} - 2454954.554702}{0.8354573} \tag{1}$$

The integer part of E is the epoch and the decimal part of E is the phase.

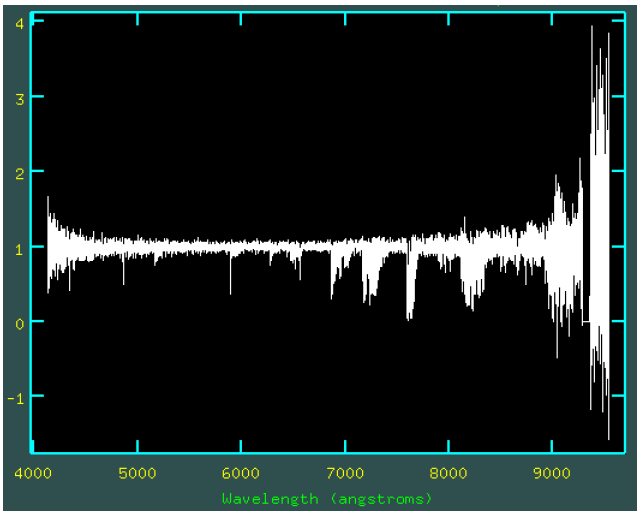

Figure 2. Example spectrum (Spectrum 4) obtained by the Mayall Telescope on September 26, 2010. The spectrum has been reduced and normalized.

Spectrum Number	Julian Date	Phase
1	2455465.63409722	0.736
2	2455465.73430057	0.856
3	2455465.79096064	0.924
4	2455465.8518264	0.997
5	2455466.81974781	0.155
6	2455467.80578357	0.336
7	2455467.83015266	0.365

Table 2. List of Spectra along with the Julian Date and phase of observation.

3. RADIAL VELOCITY MEASUREMENTS

Radial velocity measurements were obtained using the FXCOR task in *IRAF* (Tody 1986). FXCOR is based off the Fourier cross-correlation method developed by Tonry & Davis (1979). An overview of FXCOR functionality and commands is given by Alpaslan (2009). FXCOR uses a template of known redshift to determine the shift in another spectrum. If one of the spectra is obtained during an eclipse, it can be used as a template. During an eclipse there is no radial motion of the individual stars and therefore there is no shift in the atomic lines (except for the shift due to the movement of the entire system, discussed shortly). Spectrum 4 was obtained during a phase of 0.997 (during the primary eclipse) and was thus utilized as the template to measure the shifts for the other spectra. By using one of the obtained spectra as a template, the systemic velocity cannot be determined, however, this information is not important for determining system parameters through binary analysis.

Each spectra was divided into 200 Å regions and analyzed with FXCOR. The regions beyond 7000 Å were excluded as they are dominated by telluric interference. After running FXCOR on each range, the radial velocities were averaged and the standard deviation was calculated. Each run of FXCOR returns an observed velocity (VOBS) and a true velocity (VHELIO). The VHELIO measurement includes the heliocentric correction and thus represents the actual velocity of the stars. Therefore, for each wavelength range, the VHELIO measurement was recorded. Out of the seven obtained spectra, two radial velocities and corresponding errors were obtained for four of them. The results are displayed in Table 3. Spectrum 4 was used as a template and thus could not be used to obtain measurements. Spectrum 3 was obtained at a phase of 0.924 and thus the atomic lines were severely blended. FXCOR could not determine two distinct radial velocity measurements for this spectrum and instead returned a broad correlation peak centered on a velocity of zero. Since FXCOR could not be used to distinguish two velocities, Spectrum 3 was excluded. The severe blending of the atomic lines makes determining radial velocities through FXCOR impossible for Spectrum 3. Through the FXCOR analysis of Spectrum 7, the different wavelength ranges returned drastically different shifts,

indicated by the large standard deviations listed in Table 3. Certain ranges reported two negative velocities and since we are using Spectrum 4 as a template, this is not physically possible. Due to the inconsistencies in the returned radial velocities, Spectrum 7 was excluded.

Spectrum Number	Radial Velocity (km/s)	Standard Deviation (km/s)
1	-157.976 122.754	11.988 8.477
2	-114.290 113.457	23.945 15.798
3	- -	- -
4	- -	- -
5	-118.871 127.581	13.512 12.527
6	-115.685 144.144	13.207 24.092
7	10.874 -168.960	102.131 69.858

Table 3. Radial velocities determined using FXCOR. Spectrum 3 was excluded due to severely blended correlation peaks. The results of Spectrum 7 are listed but were excluded in analysis due to the poor results. Spectrum 4 was used as a template and thus could not be used to determine radial velocities.

4. BINARY ANALYSIS

The binary analysis was conducted in *PHOEBE* (PHysics Of Eclipsing BinariEs) (Prša & Zwitter 2005). The first task was to build a forward model. The values reported in the literature were inputted as initial values, including the inclination, mass ratio, fillout factor and temperature ratio listed in Table 1. These initial values alone do not produce a well fitting light curve. The initial light curve model using the values reported in the literature is displayed in Figure 4. The semi-major axis of the system was initially set by visually inspecting the radial velocity curve. The semi-major axis value was varied until the radial velocity curve included the radial velocity measurements. Throughout the binary analysis, the eccentricity was assumed to be zero. Due to the close proximity of the stars in contact binaries, their orbits have circularized (Prša et al. 2011). With the initial values, optimizers were run to refine the system parameters. The parameters were optimized using the Nelder-Mead solver. The Nelder-Mead method of minimization was first proposed by Nelder & Mead (1965) however, the *PHOEBE* optimizer utilizes a wrapper on scipy.optimize, which utilizes the algorithm developed by Gao & Han (2012). The Nelder-Mead optimizer is often called the simplex method since it utilizes simplexes to minimize a function. In 2-dimensions, the algorithm utilizes a triangle. The value of the function is computed at each vertex and the maximum vertex is selected. A line is then drawn through the vertex and the center of the opposite face. The lowest value on this line is found and the maximum vertex is moved to this location. The process is then repeated many times. For higher dimensions, the process is the same except a simplex, or the higher-dimensional analog of a simplex, is used.

Since the radial velocity curve only consists of 4 data points for each star, when running optimizers they contribute little to the overall optimization if conducted with the light curve and radial velocity curve together. Essentially, since the light curve contains many more data points than the radial velocity curve, the radial velocity measurements are "overlooked" by the optimizer. Therefore, radial velocity parameters (including mass ratio and semi-major axis) were optimized using just the radial velocity curve. These values were then fixed and the other system parameters were optimized using the light curve and the radial velocity curve. Overall, the optimized values are inclination, mass ratio, fillout factor, temperature ratio and semi-major axis. Table 4 displays the optimized values for these parameters compared to the initial values. Figure 3, 4 and 5 display the model outputs created using these optimized parameters including a mesh plot, a light curve and a radial velocity curve.

Parameter	Literature Value	Optimized Value
Inclination	77.788°	72.475°
Mass Ratio	0.81789	0.83154
Fillout Factor	0.18943	0.042579
T_{eff} Ratio	0.97814	0.96036
Semi-Major Axis	-	4.9534 $R_\odot$

Table 4. List of optimized values compared to the initial values. There is no reported value for semi-major axis in the previous study by Prša et al. (2011).

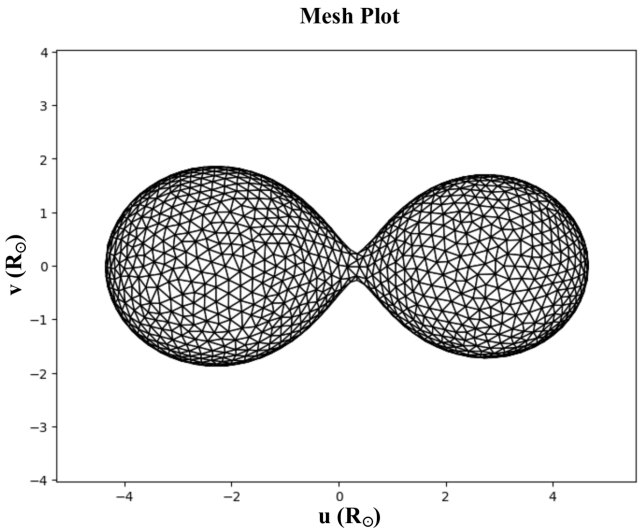

Figure 3. Graphic representation of KIC 7766185 displayed face on at a phase of 0.25. This model demonstrates the "peanut" shape of contact binaries discussed in Section 1.

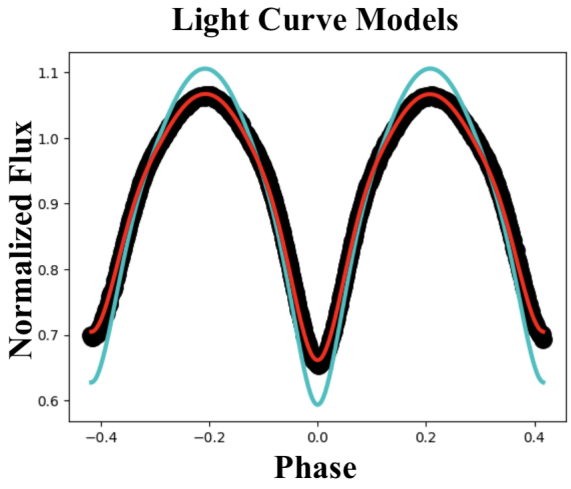

Figure 4. *Kepler* light curve (black data points), the model light curve created using the optimized values (red line) and the model light curve created using the literature values (blue line). The improvement through the Nelder-Mead Optimizer is apparent.

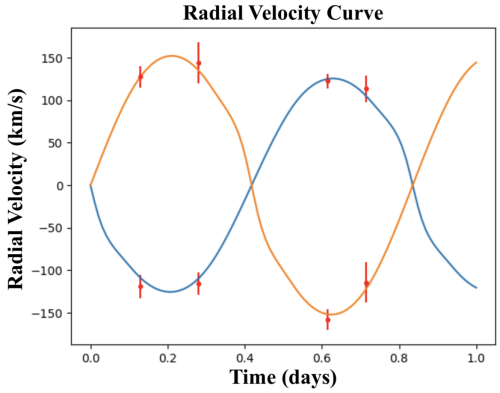

Figure 5. Radial velocity measurements (red data points) along with the model radial velocity curves created using the optimized parameters.

For the light curve parameters, only the Nelder-Mead Optimizer was used to refine the values from the previous literature. For the radial velocity curve analysis, Markov Chain Monte Carlo (MCMC) Sampling was conducted. A future work which will be conducted by the author includes utilizing MCMC sampling to further refine and produce appropriate error ranges for the light curve parameters. A pedagogical review of MCMC sampling is given in Hogg & Foreman-Mackey (2018). MCMC is used to sample probability density functions (PDFs). Specifically, MCMC is used to randomly sample the posterior PDF ($p(\theta|D)$), or the PDF for the parameters (θ) given the data (D). A set of prior distributions may also be added to the sampler if there is any prior knowledge on a parameter, such as a reliable estimate from the literature. This sampling gives appropriate errors on system parameters and further refines the parameter values. *PHOEBE* utilizes the MCMC sampler *emcee* developed by Foreman-Mackey et al. (2013).

The parameters sampled were the mass ratio and $a \sin i$. The MCMC sample was run with 16 walkers for 3000 iterations. Convergence occurs when the parameter space has been sampled thoroughly to produce appropriate error ranges on parameters. To assess convergence, corner plots and log probability plots were analyzed. Corner plots are used to observe the posterior distributions. If convergence is reached, the distributions should be complete Gaussians. The log probability plot computes the natural log of the probability for each walker at each iteration (while the computation is ln probability, the quantity is generally written as log probability). The probability encompasses both the likelihood (i.e., how well the model explains the data) and the prior distributions. At each iteration, the mean log probability is plotted with a spread of one standard deviation. For convergence, after the burn-in, the log probability plot should show no upward or downward trends, only a random spread around a central value. If a log probability plot displays trends then more iterations are required. Figure 7 displays the corner plot and the log probability plot for the MCMC run. Both plots show the requirements for convergence.

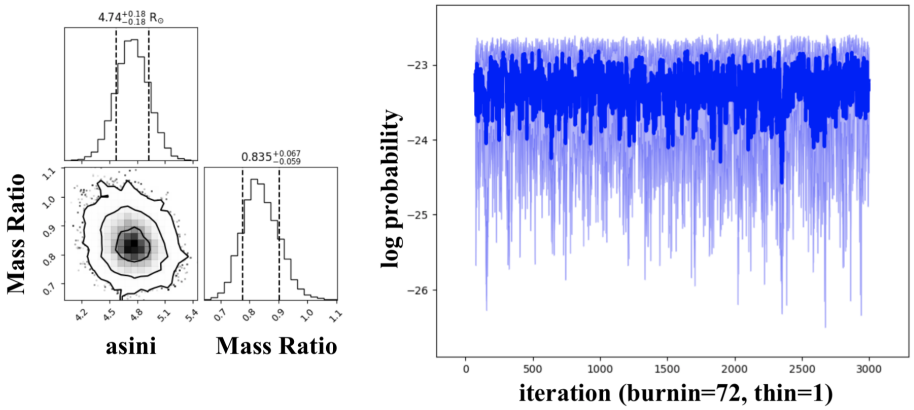

Figure 6. Corner plots (left) and log probability plot (right). For the log probability plot, the dark blue line represents the mean log probability value while the light blue is a one-sigma spread.

The system parameters for KIC 7766185 determined in this study are presented in Table 5. The table first displays the light curve parameters which were determined from the Nelder-Mead Optimizer. Since only the optimizer was used on the light curve, appropriate error ranges cannot be assigned to the light curve parameters. A future work will include conducting MCMC on the light curve. The second half of the table displays radial velocity parameters which have appropriate error ranges from MCMC sampling. The error ranges are based on a one-sigma range.

Parameter	Value
Light Curve Parameters	
Fillout Factor	0.042579
inclination	72.475^{o}
T_{eff} Ratio	0.96036
$R_{equiv,\ primary}$	$1.9864\ R_{\odot}$
$R_{equiv,\ secondary}$	$1.8287\ R_{\odot}$
Radial Velocity Curve Parameters	
Mass Ratio	$0.835^{+0.067}_{-0.059}$
$a \sin i$	$4.74 \pm 0.18\ R_{\odot}$
semi-major axis*	$4.97^{+0.19}_{-0.18}\ R_{\odot}$
$M_{primary}$	$1.29^{+0.19}_{-0.15}\ M_{\odot}$
$M_{secondary}$	$1.08^{+0.13}_{-0.12}\ M_{\odot}$
Ω*	$3.46^{+0.11}_{-0.1}$

Table 5. System parameters of KIC 7766185 determined from this study.
* Ω is the dimensionless Roche potential of the common envelope from the primary star's reference.
* The value for semi-major axis was obtained using the inclination determined from the light curve study and the $a \sin i$ value and error ranges determined from MCMC sampling.

5. PERIOD STUDY

To determine any period variations of KIC 7766185, an O-C diagram (also known as an eclipse timing variation diagram) was constructed. To verify if there have been any changes in the period reported by *Kepler*, the *TESS* observations were analyzed. Using the *TESS* Sector 14 light curve, the times of minima for the primary eclipse were measured using the Find Extremum function in *Peranso*. O-C is the observed time of eclipse minus the calculated time of eclipse, which is calculated with the following equation:

$$O - C = T_{obs} - (T_0 + nP) = T_{obs} - (2454954.554702 + n * 0.8354573) \quad (2)$$

Where T_{obs} is the observed time of eclipse in days, T_0 is the ephemeris in days, n is the current epoch and P is the period in days. The ephemeris and period value were obtained from the *Kepler Eclipsing Binary Catalog*. The O-C diagram is displayed in Figure 7.

Analyzing the O-C diagram reveals no upward or downward trends. Therefore, the period throughout the *TESS* Sector 14 observations is the same as the *Kepler* period and there has been no period change between the *Kepler* measurements (2013) and the *TESS* measurements (2019). The data points consistently lie below the x-axis. This indicates that the ephemeris value provided by the *Kepler Eclipsing Binary Catalog* needs refinement. This value is $2454954.554702 \pm 0.041523$ Julian Date. The new proposed ephemeris which centers the O-C diagram on the x-axis is 2454954.55433995 Julian Date, which lies within the error range of the old value. Using this value for ephemeris centers the data points around an O-C value of zero (Figure 8).

6. DISCUSSION

This study conducted the first in-depth binary analysis of KIC 7766185 using both photometric and spectroscopic observations. Compared to the values reported in Prša et al. (2011) (see Table 1), the values determined for mass ratio and temperature ratio are in good agreement, with a percent difference of 2.07% and 1.84% respectively. The values determined for inclination deviates from the reported data with a percent difference of 7.07%. The largest deviation from the literature is the fillout factor. The determined value (0.04257) has a percent difference of 126.59% from the value reported in Prša et al. (2011) (0.18943). These results demonstrate the importance of in depth studies of contact

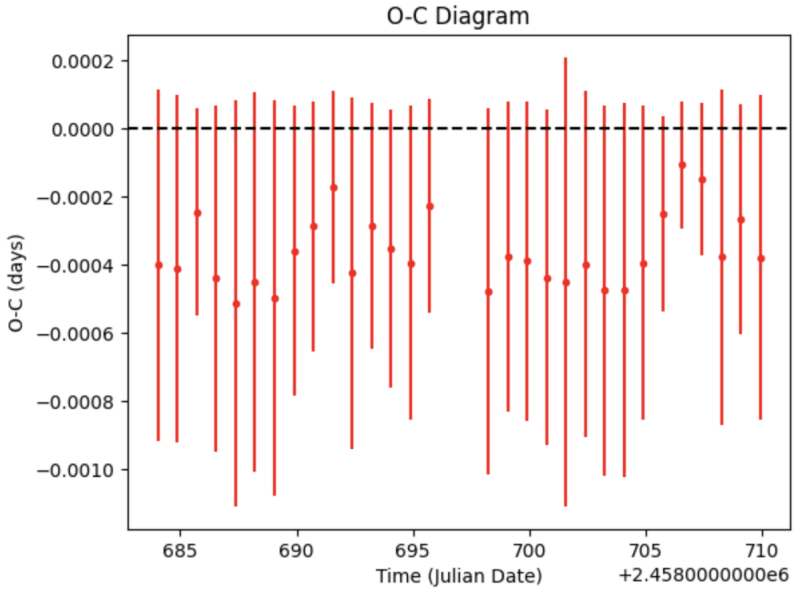

Figure 7. O-C diagram created using the *TESS* light curve

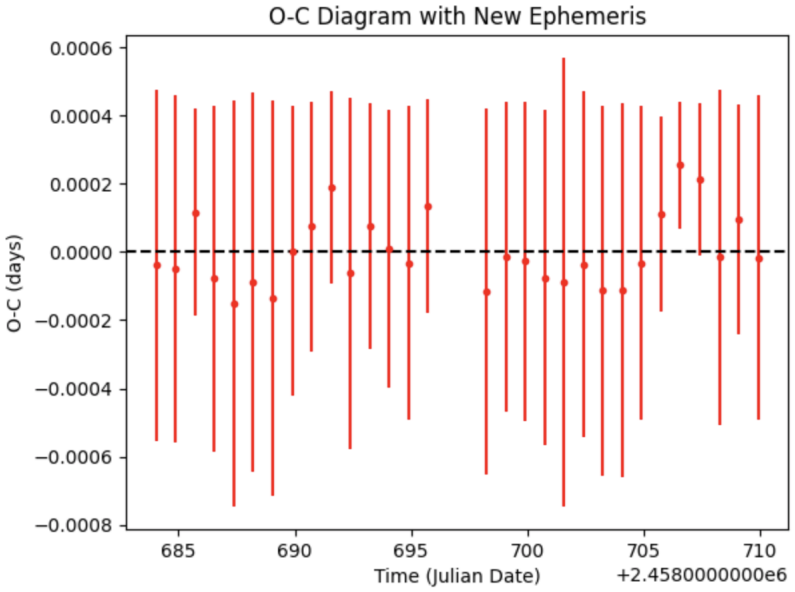

Figure 8. O-C diagram created using the updated ephemeris of 2454954.55433995 Julian date

binaries to not only determine absolute parameters, but to refine the parameters reported in large pipeline studies. The light curve models displayed in Figure 4 clearly display how the use of optimizers refines the parameter values to better fit the observations.

From the binary analysis, the sub-type of KIC 7766185 is determined. Since we do not have multiple light curves in multiple filters, the absolute temperature of both stars cannot be determined. However, by using the *Kepler* temperature, we can confirm that KIC 7766185 is not a B-type system. If we take the primary temperature to be the *Kepler* temperature of 5977 K, then the secondary temperature is 5740 K. The temperature difference is 237 K. While the temperature reported by *Kepler* is not reliable as a primary temperature (see the end of Section 1), it can be used

to rule out KIC 7766185 as a B-type system. As stated in Csizmadia & Klagyivik (2004), B-type systems typically have a temperature difference of greater than 1,000 K. With a temperature ratio of 0.96036, the primary temperature would have to be 25,227 K (a nonphysical value for this system) before the temperature difference between the primary and secondary becomes greater than 1,000 K. Therefore, KIC 7766185 is not a B-type system and the stars are in thermal contact.

KIC 7766185 is an A-type W UMa system. A-Type systems occur when the hotter star is the larger star (Csizmadia & Klagyivik 2004). The temperature ratio is defined as T_2/T_1, therefore, with a value of 0.96036, the primary (T_1) is hotter. The equivalent radius of the primary (1.9864 $R_\odot$) is larger than the equivalent radius of the secondary (1.8287 $R_\odot$). Therefore, the primary star is the hotter and larger component, verifying KIC 7766185 as an A-type W Uma star.

The period analysis did not determine any period variations for KIC 7766185. One motivation of this section was to determine if KIC 7766185 is a red nova candidate. However, analysis of the O-C diagram (Figure 7) reveals no period changes between the *Kepler* and *TESS* observations. Therefore, as of now, KIC 7766185 is not a red nova candidate. However, the time between the *Kepler* and *TESS* observations (6 years) is short compared to the lifetime of these stars. Therefore, the lack of a determined period variation may be due to the short time span between observations. If future studies conduct additional photometric observations, the O-C diagram should be extended to continue the search for period fluctuations. The data points in the O-C curve lie below the x-axis, indicating that the ephemeris reported in the *Kepler Eclipsing Binary Catalog* should be updated. This study determines a value of 2454954.55433995 Julian Date for the new ephemeris of KIC 7766185.

7. CONCLUSION

This study conducted the first photometric and spectroscopic study of KIC 7766185. Spectra obtained from the Mayall 4-m telescope were resolved into radial velocity measurements. The radial velocity curve and the *Kepler* light curve were used in *PHOEBE* to perform binary analysis. This study determined the first set of absolute stellar parameters for KIC 7766185. These parameters confirm the system as an A-type W UMa star. The period analysis determined no period variations between the *Kepler* and *TESS* observations. As of now, KIC 7766185 is not a red nova candidate since no period decay was discovered. Future observations are needed to determine the absolute temperatures of KIC 7766185. Photometry in multiple filters will allow the determination of primary and secondary effective temperatures, which can be appended to the list of absolute parameters determined by this study. A future study will conduct MCMC sampling on the light curve to obtain appropriate error ranges on the light curve parameters.

8. ACKNOWLEDGEMENTS

The author would like to thank Dr. Scott Engle, Dr. Angela Kochoska and Dr. Andrej Prša from the Villanova Department of Astronomy and Planetary Science for continuous support and guidance throughout this project. The author would also like to thank Dr. Jerome Orosz from the San Diego State University Department of Astronomy for answering questions about the spectroscopic reduction process.

REFERENCES

Alpaslan, M. 2009, arXiv e-prints, arXiv:0912.4755

Binnendijk, L. 1965, Veroeffentlichungen der Remeis-Sternwarte zu Bamberg, 27, 36

Borucki, W. J., Koch, D., Basri, G., & et al. 2010, Science, 327, 977, doi: 10.1126/science.1185402

Brown, A. G. A., Vallenari, A., Prusti, T., et al. 2021, Astronomy & Astrophysics, 649, doi: 10.1051/0004-6361/202039657

Brown, T. M., Latham, D. W., Everett, M. E., & Esquerdo, G. A. 2011, AJ, 142, 112, doi: 10.1088/0004-6256/142/4/112

Csizmadia, S., & Klagyivik, P. 2004, Astronomy & Astrophysics, 426, 1001–1005, doi: 10.1051/0004-6361:20040430

Eker, Z., Demircan, O., & Bilir, S. 2008, Monthly Notices of the Royal Astronomical Society, 386, 1756–1758, doi: 10.1111/j.1365-2966.2008.13155.x

Foreman-Mackey, D., Hogg, D. W., Lang, D., & Goodman, J. 2013, Publications of the Astronomical Society of the Pacific, 125, 306, doi: 10.1086/670067

Frasca, A., Molenda-Zakowicz, J., De Cat, P., et al. 2016, A&A, 594, A39, doi: 10.1051/0004-6361/201628337

Gao, F., & Han, L. 2012, Computational Optimization and Applications, 51, 259, doi: 10.1007/s10589-010-9329-3

Gazeas, K., & Stępień, K. 2008, Monthly Notices of the Royal Astronomical Society, 390, 1577, doi: 10.1111/j.1365-2966.2008.13844.x

Gazeas, K. D., Loukaidou, G. A., Niarchos, P. G., et al. 2021, Monthly Notices of the Royal Astronomical Society, 502, 2879–2892, doi: 10.1093/mnras/stab234

Høg, E., Fabricius, C., Makarov, V. V., et al. 2000, A&A, 355, L27

Hogg, D. W., & Foreman-Mackey, D. 2018, The Astrophysical Journal Supplement Series, 236, 11, doi: 10.3847/1538-4365/aab76e

KPNO. 2021, Mayall Telecope Parameters, http://www-kpno.kpno.noao.edu/kpno-misc/mayall_params.html

Lucy, L. B. 1968, Astrophysical Journal, 151, 1123, doi: 10.1086/149510

Nelder, J. A., & Mead, R. 1965, The Computer Journal, 7, 308, doi: 10.1093/comjnl/7.4.308

Paunzen, E., & Vanmunster, T. 2016, Astronomische Nachrichten, 337, 239, doi: 10.1002/asna.201512254

Prša, A., Batalha, N., Slawson, R. W., et al. 2011, The Astronomical Journal, 141, 83, doi: 10.1088/0004-6256/141/3/83

Prša, A., Guinan, E. F., Devinney, E. J., et al. 2008, ApJ, 687, 542, doi: 10.1086/591783

Prša, A., & Zwitter, T. 2005, Astrophysical Journal, 628, 426, doi: 10.1086/430591

Ricker, G. R., Winn, J. N., Vanderspek, R., et al. 2015, Journal of Astronomical Telescopes, Instruments, and Systems, 1, 014003, doi: 10.1117/1.JATIS.1.1.014003

Ruciński, S. 1986, Symposium - International Astronomical Union, 118, 159–172, doi: 10.1017/S0074180900151307

Rucinski, S. M. 1982, A&A, 112, 273

Terrell, D., Gross, J., & Jr, W. 2012, The Astronomical Journal, 143, 99, doi: 10.1088/0004-6256/143/4/99

Tody, D. 1986, in Instrumentation in Astronomy VI, ed. D. L. Crawford, Vol. 0627, International Society for Optics and Photonics (SPIE), 733 – 748. https://doi.org/10.1117/12.968154

Tonry, J., & Davis, M. 1979, AJ, 84, 1511, doi: 10.1086/112569

Tylenda, R., Hajduk, M., Kamiński, T., et al. 2011, Astronomy & Astrophysics, 528, A114, doi: 10.1051/0004-6361/201016221

Valdes, F. 1992, in Astronomical Society of the Pacific Conference Series, Vol. 25, Astronomical Data Analysis Software and Systems I, ed. D. M. Worrall, C. Biemesderfer, & J. Barnes, 417